The magnetic and crystalline structure of the Laves phase superconductor $CeRu_2$

1997 J. Phys.: Condens. Matter 9 4185

(http://iopscience.iop.org/0953-8984/9/20/017)

J. Phys.: Condens. Matter **9** (1997) 4185–4195. Printed in the UK PII: S0953-8984(97)81209-X

The magnetic and crystalline structure of the Laves phase superconductor $CeRu_2$

A Huxley†, J X Boucherle†, M Bonnet†, F Bourdarot†, I Schustler†, D Caplan†, E Lelievre‡, N Bernhoeft‡, P Lejay§ and B Gillon‖

† CEA, Département de Recherche Fondamental sur la Matière Condensée, SPSMS, Grenoble 38054, France

‡ Institut Laue–Langevin, Grenoble, France

§ Centre de Recherche sur les Très Basses Températures, CNRS, Grenoble, France

‖ CEA, Laboratoire Léon Brillouin, Saclay, France

Received 22 January 1997

Abstract. We report measurements of the field-induced magnetization density in $CeRu_2$. The main results of the study are that the magnetic density is located equally at the Ce and Ru sites, and that the distribution of the induced magnetization about the Ce site extends to larger distances than predicted for Ce^{3+} ions with well localized f electrons. Our measurements also cover the superconducting state, where we do not observe any suppression of the spin susceptibility. In an accompanying structural study (in zero field) of our single crystal we detect a small deviation from the ideal Laves phase structure. These results are discussed in relation to the unusual electronic and magnetic properties of this compound.

1. Introduction

$CeRu_2$ is a clean type II superconductor with a critical temperature of 6.15 K. Recent studies have also concluded that very weak static magnetic moments may exist below 40 K [1, 2] which persist into the superconducting state. It provides an interesting addition to the growing family of f-electron superconductors which show unusual magnetic and superconducting properties.

$CeRu_2$ has been conventionally assigned to have the cubic Laves phase structure [3]. In this structure all of the Ce sites and likewise all of the Ru sites are equivalent. The Ru forms a three-dimensional open network of corner-sharing tetrahedra interpenetrated by a diamond structure of Ce atoms. The Ce–Ce distance is compressed, whereas the Ru–Ru and Ce–Ru separations are standard. It is the close proximity of the Ce atoms that differentiates the Ce Laves phase compounds (with the exception of $CeAl_2$) from the majority of Ce alloys: it favours the delocalization of the Ce f electrons in preference to the formation of large localized magnetic moments.

$CeRu_2$ is usually classified as an intermediate-valence compound. High-energy spectroscopic studies have been interpreted as demonstrating the existence of an f-electron component of the density of states below the Fermi surface [4]. The small Ce radius deduced from the lattice parameter, rather than indicating the f levels to be empty (i.e. a Ce^{4+} ion) [5], indicates that the occupied f levels must be strongly hybridized. This is confirmed by band-structure calculations [6–9], which assume that all of the f electrons are delocalized, and conclude that the electronic density of states (DOS) at the Fermi surface is

0953-8984/97/204185+11$19.50

made up principally from Ce 4f and Ru 4d electrons, with approximately one f electron/Ce below the Fermi surface. The calculated Fermi surfaces agree well with recent quantum oscillatory measurements [10]. Agreement between the different calculations of the DOS close to E_F and experiment is however less consistent: the calculation of the DOS is sensitive to the quality of the approximations used to treat many-body effects.

Recent work concerning superconductivity has focused on an abrupt change in the superconducting mixed state at an applied field H^* ($H_{c1} \ll H^*$ (T) $\ll H_{c2}$) from a reversible magnetic behaviour at low fields ($H < H*$) to an irreversible behaviour at high fields ($H > H^*$) [11–20]. While this change can be explained by a continuous evolution of the rigidity of the flux-line lattice and the collective action of weak flux-line pinning centres [21], it has been suggested that alternatively a true phase transition might occur. Such a transition might involve a change in the underlying electronic structure [22], or a change in the symmetry of the superconducting state. In particular, attention has been paid to the possibility of a transition to a modulated (Fulde–Ferrell–Larkin–Ovchinnikov) superconducting state [23–26]. Knowledge of the microscopic pinning mechanism is clearly vital for testing our understanding of the above phenomena. The origin of the static magnetism and its possible role in pinning the flux-line lattice have to be determined. For a detailed understanding of the flux pinning it is also essential to identify the characteristic metallurgical defects. The present study of the crystallography and magnetic form factors of a single crystal provides a foundation for the examination of the above issues.

In the next section (section 2) we give some details of our sample and the apparatus used. In section 3 we present the structural investigation of our crystal: the crystal structure is found to differ slightly from that of an ideal Laves phase. The magnetization density determined in the normal state is discussed in section 4, with particular attention paid to the Ce form factor. In section 5 we discuss our measurements for the superconducting state, where we do not detect an expected decrease in the magnetization density. The significance of the above results is discussed in section 6.

2. Experimental details

All of the measurements were performed on the same unannealed single crystal of mass 1.7 g, grown by the Czochralski method in a tri-arc furnace. Its static magnetic susceptibility is almost temperature independent. A small increase at low temperature contributes less than 10% to the total susceptibility and is most probably due to defects. If this contribution is modelled by a Curie–Weiss term and attributed to free Ce^{3+} moments ($\mu_{Ce}^{3+} = 2.54\ \mu_B$), its magnitude corresponds to a ratio of less than 5×10^{-4} Ce^{3+}/Ce atom. The zero-field ac susceptibility has been previously reported [1]. It shows a small anomaly just above 40 K, below which the susceptibility increases. The temperature of 40 K coincides with the appearance in zero field of static magnetic moments inferred by muon-spin-relaxation (μSR) measurements in a different polycrystalline specimen. The μSR measurements require the observed depolarization to come from at least 15% of the sample, and cannot be explained by a contribution from a segregated second phase.

The polarized neutron experiments were done at the polarized neutron diffractometers 5C1 (Laboratoire Léon Brillouin, CEA, Saclay) at a maximum applied field of 5 T, and D3 (Institut Laue–Langevin, Grenoble), at a maximum applied field of 4.6 T. Both instruments measure diffracted intensities for neutrons ($\lambda = 0.843$ Å) alternately polarized parallel and anti-parallel to an applied field. Our crystal was oriented with a [110] axis parallel to the field direction, and only Bragg peaks in the scattering plane perpendicular to this were examined. The data from the two diffractometers are consistent.

The diffraction data for the crystallographic analysis were recorded on the D15 three-circle diffractometer (Institut Laue–Langevin, Grenoble) with the same sample configuration and a nearly identical incident wavelength ($\lambda = 0.8563$ Å).

3. Crystallography

$CeRu_2$ has conventionally been assigned as having the Laves phase structure, which is face-centred cubic with the space group $Fd\bar{3}m$ (*International Tables* No 227).

In a preliminary study of another similarly prepared $CeRu_2$ single crystal with an x-ray precession camera, diffraction spots at the Bragg positions $(2 + 4n, 0, 0)$ and $(2 + 4n, 4n', 4n'')$ were observed ($n' \neq 0, n'' \neq 0$). The former reflections are generally forbidden by the crystal space group, while the latter are forbidden for the particular choice of atomic coordinates appropriate to the ideal Laves phase structure. The aims of our neutron diffraction study were (i) to extract the extinction parameters for our crystal, needed for the analysis of the polarized neutron data, and (ii) to look for the presence of the above 'forbidden' peaks and thus test whether the assignment of the ideal Laves phase crystal structure is in fact accurate.

Data were taken for the first 120 Bragg peaks in the [110] zone of the nominal Laves phase structure, and for the first few positions in each of the above series of 'forbidden' peaks, with ten times the counting period.

We were able to detect both of the above types of 'forbidden' peak in our neutron study. They are weak compared to the strongest Bragg peaks, but too intense to be explained by a $\lambda/2$ contamination of the incident beam. We also found no intensity at the peak positions, which are more generally disallowed for an FCC structure.

The presence of the $(2 + 4n, 4n', 4n'')$ reflections can be explained by considering an anisotropic Debye–Waller factor for the Ru atoms. This is consistent with the usual Laves phase crystal symmetry, since the Ru are not at sites of local cubic symmetry. The fitted Debye–Waller factor is comparable in magnitude to the value estimated from the Debye temperature ($\theta_D = 172$ K [11]) and can therefore be taken to represent phonon displacements. The Ru atoms form a network of corner-sharing tetrahedra (figure 1). The observed anisotropy then implies that in each tetrahedron the Ru vibrates over a distance which is 30% larger in a plane parallel to the opposite face of the tetrahedron than in the perpendicular direction. A consequence is that the bulk modulus should be large relative to the shear modulus. This conclusion is confirmed by recent measurements of the elastic constants [27].

The $(2+4n, 0, 0)$ reflections, however, cannot be explained with an anisotropic Debye–Waller factor, and require the adoption of a symmetry group that is less symmetric than that for the ideal Laves phase structure. The natural choice is to consider the group $F\bar{4}3m$ (*International Tables* No 216), which allows the above reflections, but preserves all of the other FCC reflection conditions. For this choice, alternate Ru tetrahedra are enlarged and compressed (figure 1), leaving the positions of the Ce unchanged. While all of the Ru atoms still have identical environments, the Ce environments are then divided into two types, Ce I and Ce II. The resulting structure would then permit the existence of anti-phase domains, corresponding to whether a particular Ce in the original Laves phase cell is allocated to a Ce I or Ce II site. The choice of origin determines the sign of the scattering lengths for the $(2 + 4n, 0, 0)$ reflections.

The fit to the integrated intensities (figure 1) is improved dramatically when the above reduction of symmetry is permitted, while the mean displacements of the Ru required amount to only 0.14% of the unit-cell parameter, compared to 1% for the phonon smearing at room

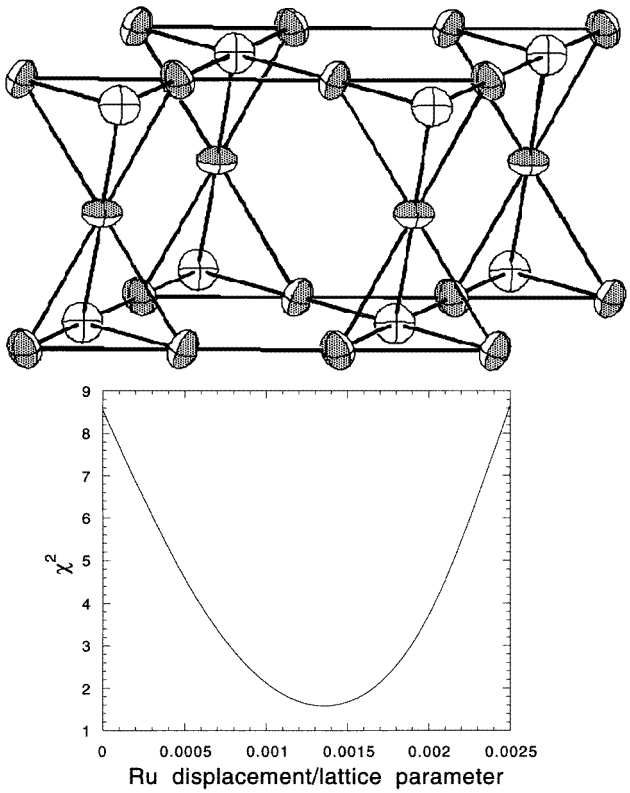

Figure 1. A section of the structure of $CeRu_2$: only Ru atoms have been drawn for clarity. The lines joining adjacent Ru atoms are crystalline ⟨[110]⟩ directions. The angular anisotropy of the thermal mean square displacements of the Ru ions is represented schematically by ellipses, the shaded faces of which indicate the directions of additional static displacements away from the ideal Laves phase structure. The weighted mean of the squared differences between the observed peak intensities and those fitted, χ^2, is also shown, as a function of the displacement of the Ru ions. The quality of the fit is significantly improved for a small displacement of the Ru of magnitude 0.14% of the lattice parameter.

temperature. The extinction is determined by the mosaic spread, which is found by fitting to be $d\Omega = 24$ seconds of arc.

The profile of the [600] ray, which is forbidden for the $Fd\bar{3}m$ Laves phase structure, is shown in figure 2. This ray, which is representative of the other $(2+4n, 0, 0)$ Bragg peaks, comprises a sharp peak of the same width as the standard Bragg peaks (which is equal to the instrumental resolution), superimposed on an additional more diffuse peak. Both of these contributions are included in the integrated intensities that we used to perform the least-squares refinements referred to in the preceding paragraph. The diffuse scattering, if fitted to a Gaussian line shape, would correspond to a correlation radius in real space of about 20 Å, which is much smaller than the minimum mosaic block size compatible with the extinction coefficients.

Since the scattering lengths for the two allowed anti-phase domains have opposite magnitudes and therefore average to zero, a finely interspersed structure comprised equally of the two types of domain would not be consistent with the observation of a sharp Bragg peak. Therefore the partition of the sample into the two anti-phases is either not

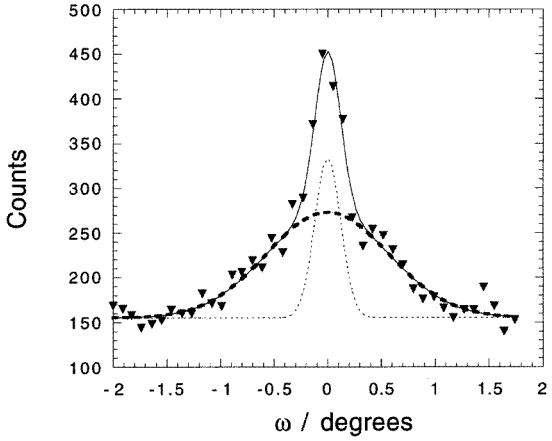

Figure 2. The peak profile of the 600 Bragg peak, which is forbidden for the ideal Laves phase structure, is shown as a function of the rocking angle ω. The peak contains two components (represented by the broken lines): (i) a narrow component with a width equal to the instrumental resolution and (ii) a diffuse component. The solid line is the sum of these two contributions.

homogeneous, or the domains are relatively large. In both cases the boundaries between two anti-phase domains would create strain fields, and these could also contribute to the diffuse scattering (Huang scattering). The diffuse peak might then be relatively intense, because the displacements due to strain could be of the same order of magnitude as those giving rise to the original distortion from the Laves phase structure.

The following analysis of the magnetic form factors is found to be insensitive to the small deviations from the ideal Laves phase structure reported above. Different moments on the two Ce sites are permitted for the more general $F\bar{4}3m$ space group. We have considered such a possibility; the moments refine to almost identical values, and the quality of the fit to the data is not improved.

4. The magnetic form factors in the normal state

By far the most significant contribution to the neutron scattering amplitude, $\bar{b}$, does not depend on the direction of the neutron polarization, and is principally of nuclear origin. For our experimental geometry (for which the neutron polarization is perpendicular to the scattering plane), spin-flip processes do not occur. There are nevertheless further small contributions to the scattering amplitude, denoted by p, which change sign according to the direction of the neutron polarization. From the ratio of the neutron cross-sections for the two neutron polarizations, $R = (\bar{b} + p)^2/(\bar{b} - p)^2 \approx 1 + 4p/\bar{b}$ (assuming $p \ll \bar{b}$), one can deduce the polarization-dependent component p. The contributions to p originate from magnetic scattering, and a term related to spin–orbit scattering due to the interaction between the electric field distribution in the sample and the moving neutron. A further contribution from nuclear moments does not occur if the temperature is sufficiently high that the nuclear moments are not aligned by the applied field. The spin–orbit contribution to p is independent of the applied field, and changes sign according to whether the scattering is to the right or left of the incident beam. Its magnitude can be estimated from tabulated values of the electronic form factors, which confirm that it is too small to contribute significantly to our measurements. Its contribution is anyway eliminated by averaging data from the two

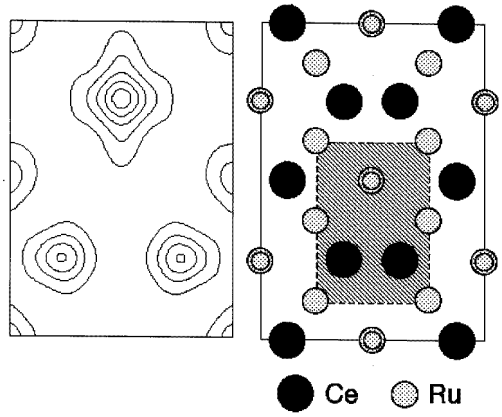

Figure 3. A contour plot of the induced magnetization density (a maximum-entropy reconstruction determined from the experimentally measured magnetic scattering lengths) is shown, projected onto a $[1\bar{1}0]$ crystal direction. The area projected corresponds to that shaded in the projected structure (right-hand panel); the double concentric circles represent columns with twice as many atoms per length as those depicted by single circles.

symmetric Bragg conditions to the left and right of the incident beam. The measured p thus gives the magnetic scattering amplitude. The above interpretation is valid for the kinematic theory of diffraction. Since our sample is rather large, we also take into account dynamic effects by inserting extinction parameters deduced from the refinement of the nuclear Bragg integrated intensities. Standard corrections are also made for the incomplete polarization of the neutrons.

The induced magnetization in a paramagnet can be considered to arise from two origins. The first is a diamagnetic response due to closed shells of core electrons. They give a contribution equal to about ten per cent of the measured static susceptibility in $CeRu_2$ (with opposite sign). Their contribution to the magnetic form factors can be calculated [28] from tabulated values of electron densities [29]. The second contribution consists of both orbital and spin components from incomplete shells of electrons (which may be either localized or itinerant). In the dipole approximation (valid for low-order peaks) the form factor of the unpaired electrons associated with each magnetic ion is

$$f(\kappa) \propto \mu(\langle j_0(\kappa)\rangle + \alpha\langle j_2(\kappa)\rangle)$$

with

$$\langle j_n(\kappa)\rangle = \int \mathrm{d}^3 r \; j_n(\kappa r)\Psi^2(r)$$

(where $\Psi^2(r)$ is the unpaired electron density, j_n are nth-order Bessel functions, κ is the scattering vector, α is a constant, and μ is the total moment associated with the ion). The first term, $\langle j_0(\kappa)\rangle$, arises from both orbital and spin magnetism, while the second term, $\alpha\langle j_2(\kappa)\rangle$, is uniquely due to the orbital component. To fit our data we have used the tabulated values [28] of the atomic form factors (i.e. $\langle j_n(\kappa)\rangle$ above) and the standard core-electron contributions. We obtain an excellent fit with induced paramagnetic moments, μ, of 0.000 44(2) μ_B T^{-1} associated with each cerium ion and 0.000 45(2) μ_B T^{-1} for each ruthenium ion. The coefficients α can either be taken as zero or included as free

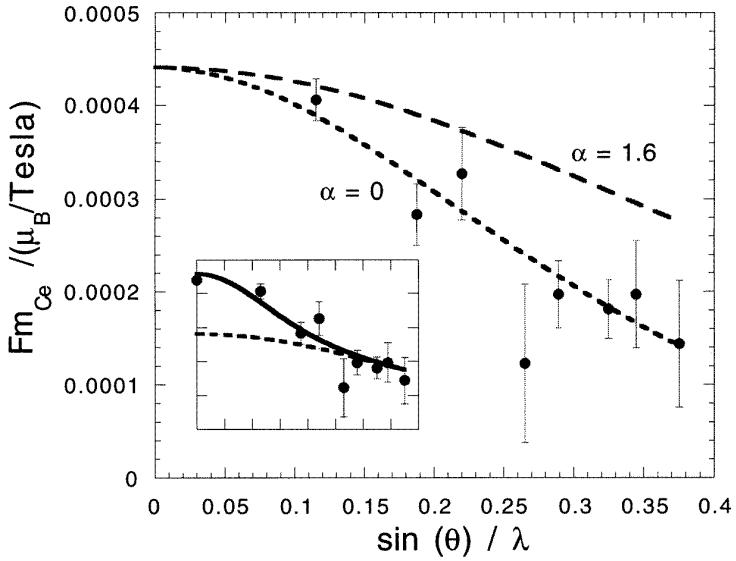

Figure 4. The Ce magnetic form factor determined from the measured scattering amplitudes (after subtraction of the diamagnetic core contribution). The point at $\sin(\theta)/\lambda = 0$ is determined from the static susceptibility. The dashed lines are the calculated curves for (i) a spin-only ($\alpha = 0$) form factor, and (ii) the standard spin + orbital ($\alpha = 1.60$) form factor for the Ce^{3+} ion, in the dipole approximation. In the inset the same data are shown. Here the dashed line corresponds to a standard ($\alpha = 1.6$) 4f-electron contribution with a magnitude scaled to give the best fit to the data above $\sin(\theta)/\lambda = 0.15$. The difference between this line and the experimental data (the solid line is a guide to the eye) might then be explained by an additional Ce 5d-electron contribution.

parameters, which then refine to $\alpha = 0.0(5)$ for Ce and $\alpha = 0.2(2)$ for Ru. The basic conclusion that the moments associated with the Ce and Ru are almost identical is not sensitive to the details of the analysis (such as the inclusion of the small diamagnetic core contributions or extinction corrections), whereas the overall magnitudes of the moments would be underestimated by about 20% if the extinction corrections were overlooked. The susceptibility due to these polarizations added to the core diamagnetism is $2.56(12) \times 10^{-4}$, which is almost identical to the total measured static susceptibility. Thus the bulk of the susceptibility is associated with a magnetization distribution localized at the Ce and Ru sites, with only a very small polarization between them. This point is illustrated by a maximum-entropy reconstruction [30] of the total magnetization density distribution (including the core diamagnetism), shown in figure 3. An anisotropy of the magnetization density around the sites, seen also in a Fourier analysis of the data, is also apparent. The magnetization densities are reduced in the directions of the nearest-neighbour ions. The usual interpretation of the anisotropy would require knowledge of the electronic configuration in the presence of the crystal field. Since for the Ru many d electrons are involved, it is unlikely that this can be unambiguously deduced from the present data alone.

For localized electrons, in the case of a strong crystal field (relative to the strength of the spin–orbit coupling) the value of α is given theoretically as $\alpha = 1 - 2/g$ where g is the Landé g-factor [31]. Such a behaviour would be typical for a transition metal element like Ru (and gives $\alpha \approx 0$). For the rare-earth elements, such as Ce, the effect of spin–orbit coupling is expected to be more important, and in this case a different value

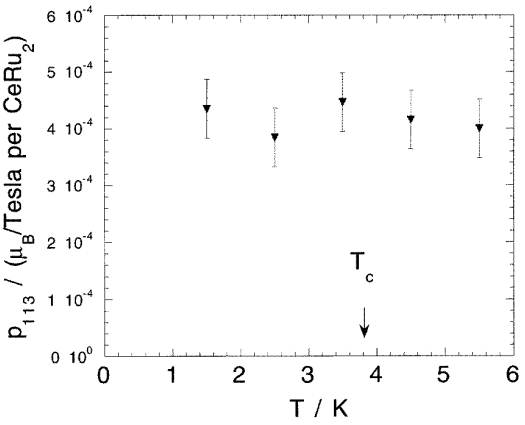

Figure 5. The magnetic scattering amplitude per $CeRu_2$ (in units of μ_B T^{-1}) for the [113] Bragg peak as a function of temperature at 3 T. The superconducting transition temperature at this field is indicated by an arrow. No change in the spin susceptibility is evident in the superconducting state.

of α is calculated. The standard value derived for the Ce^{3+} ion is $\alpha = 1.60$ [32]. The small value of α found experimentally is not consistent with this. To illustrate this point further, we have subtracted the Ru and the core contributions from the measured magnetic scattering amplitudes to determine the unpaired-Ce-electron contribution per atom for each Bragg reflection; this is plotted as a function of the scattering wave vector in figure 4. It is compared to (i) the spin-only component of the standard form factor ($\alpha = 0$) and to (ii) the standard theoretical result including an orbital contribution ($\alpha = 1.60$). The experimental data lie consistently closer to the $\alpha = 0$ curve. Physically this tells us that the induced magnetic polarization is more extended in space than is indicated by the model for localized Ce^{3+} f electrons. Deviations from the dipole approximation could occur if strong crystal-field splitting favours certain spin states of the Ce ion which break the spherical symmetry assumed in the approximation. This cannot however explain the magnitude of the spatial extent observed experimentally [33]. There are two other possibilities for explaining the discrepancy. Firstly it is possible that there is a significant contribution from Ce 5d electrons, which would be important only at the lowest values of s ($s = \sin(\theta)/\lambda$). A polarization with a conventional s-dependence could then be assigned to the 4f electrons, which would give the dominant contribution to the form factor only above $s \approx 0.15$. At the lowest values of s the contributions from the 5d and 4f electrons would be of similar magnitude (see the inset in figure 4). A second possibility is that the Ce 4f electrons do indeed behave as if their orbital angular momentum has been quenched (i.e. as described by the calculated curve with $\alpha = 0$), and that the electronic polarization has everywhere a spin-only (free-electron-like) g-factor. This would be a new and interesting result as it is contrary to what is normally found for well localized f orbitals.

In other Ce compounds, the induced moments on the Ce ions are often much larger than those on any accompanying transition metal ions [33]. In such cases the on-site repulsion of the Ce f electrons prevents the spin degeneracy of the Ce bands below the Fermi surface from being destroyed by the complete filling of the band; the Ce moments then dominate the magnetic properties. In other cases, such as that for $CeNi_5$, the Ce f levels are located above the Fermi surface and give only a minority contribution to the magnetization density

[34]. $CeRu_2$ is intermediate between these extremes; the Ce f levels extend below the Fermi surface, but they are strongly hybridized. To interpret our data further and compare them with the electronic density distribution calculated from the band structure, it is necessary to know the relationship between the magnetization density and the charge density. Taken at face value, the result that $\alpha = 0$ for both Ce and Ru in the fit to our data suggests that the conversion factor could be close to $g = 2$ everywhere. It is then possible that, as in a simple metal, the magnetic form factors give a direct measure of the contributions of the electronic weights associated with the different orbitals to the DOS at the Fermi surface (E_F). The band-structure calculations of Lopez-Aguilar *et al* [6] give the DOS at E_F as composed equally of Ce 4f and Ru 4d electrons with only a small Ce 5d-electron contribution. This is consistent with our data only if the Ce orbital moment has been quenched.

The above measurements were made at 5 K. We also made some measurements at 10 K and 100 K. At these temperatures no significant change in the magnetic structure factors relative to the data at 5 K was observed. There is therefore no significant change in the magnetization distribution on traversing the magnetic 'freezing' temperature of 40 K. This result is not inconsistent with the appearance of static magnetic moments, referred to earlier, since the absolute magnitude of the static moments is estimated as only $10^{-4}\ \mu_B$, which is within the error bars of the induced moments studied here. The result is consistent with that expected for the almost constant static susceptibility.

5. The spin susceptibility in the superconducting state

Several of the strongest magnetic scattering amplitudes were measured in a field of 3 T, as a function of temperature down to 1.5 K, to examine the superconducting state (see figure 5). The lack of any abrupt change in the magnetic scattering amplitudes near to T_c argues against a change in electronic structure, perhaps provoked by the opening of the superconducting gap. Such a change was suggested in reference [22] as a possible explanation of the irreversibility transition referred to in the introduction.

In fact, no significant change with temperature is observed (figure 5) down to the lowest temperature, whereas a decrease in the magnetic form factors has previously been observed in other s-wave superconductors [35]. The reduction is due to the singlet pairing of electrons below T_c which suppresses the Pauli spin paramagnetism. The same mechanism is also responsible for a change in the Knight shift measured by nuclear magnetic resonance (NMR) [36]. Our measurements in the normal state have shown that the form factors are almost exclusively determined by the spin polarization (the orbital and core contributions are small). The expected result would then be that the magnetic scattering amplitudes for $CeRu_2$ should fall to near zero as $T \to 0$, in the superconducting state.

While for $CeRu_2$ no detailed study of NMR in the superconducting state has been published, nuclear quadrupolar relaxation studies in zero field have been reported [37, 38]. These measurements show both a coherence peak at T_c and an exponential behaviour at low temperature in the NQR relaxation time, characteristic of an s-wave superconductor with a small gap anisotropy, and consistent with the low-temperature specific heat [11]. These observations suggest that the pairing is indeed conventional and therefore imply that it has even parity. This argues strongly against the possibility that the unchanged spin susceptibility below T_c is due to odd-parity pairing, as has been suggested for less conventional superconductors, such as UPt_3 [39].

Spin–orbit scattering is known to reduce the depression of the spin susceptibility, since such scattering breaks the time-reversal symmetry of the scattered pairs which can then be polarized. If spin–orbit scattering due to sample defects alone is responsible for the

invariant spin polarization, the spin–orbit scattering mean free path must be of the same magnitude as the coherence length [40]. The superconductivity must then be in the dirty limit. For $CeRu_2$, the fact that the Maki parameter, $\kappa_2(T)/\kappa_2(T_c)$, becomes very large at low temperature [11] indicates that the superconductivity is in the clean limit. Thus, it appears that spin–orbit scattering from metallurgical defects cannot be used to explain the constant magnetic scattering amplitudes in the superconducting state.

The above analysis is strictly applicable only for small applied fields. Our measurements were however at approximately $H_{c2}/2$. Although the spin polarization must be entirely recovered at H_{c2} (the transition at H_{c2} is second order), it has been calculated for dirty superconductors that the spin polarization is suppressed almost entirely at $H_{c2}/2$ and $T/T_c = 1/4$ (corresponding to the lowest temperature in our graph) [41]. Clearly an equivalent calculation for the clean limit is required for the present sample, which should also include the fact that $CeRu_2$ is a strongly coupled superconductor and that H_{c2} is close to the paramagnetic limiting field. A potentially more important effect concerns the flux-line lattice (FLL), which was ignored in the above calculation. While a perfectly ordered FLL might not give rise to significant extra spin–orbit scattering at $T = 0$, an imperfect FLL could, and this might offer an explanation of our data.

6. Conclusions

We have found that our single crystal has a structure slightly different from that of an 'ideal' Laves phase. The nature of the deviation is subtle; it does not directly affect the overall FCC symmetry, and the atoms are only displaced slightly from the Laves phase positions. This explains why it has not been detected in previous studies. The new structure reveals the presence of diffuse scattering which could be related to metallurgical defects. Defect sites could give rise to Ce ions with locally different environments (relatively less compressed by the surrounding Ru network). An interesting possibility is that such Ce ions, distributed randomly, might then be the source of the weak average static fields appearing below 40 K, and provide the weak-pinning centres necessary to explain the reversibility transition in the superconducting mixed state. Additionally they could explain the rather high residual resistivity (10 $\mu\Omega$ cm) and the low-temperature tail in the susceptibility of our sample. Clearly, further studies are required to identify the microscopic character of the defects. The effect of annealing on the distribution of the structural displacements could be especially interesting.

Our polarized neutron data show that the induced magnetization density is almost equally distributed around the Ce and Ru sites. The two contributions together give an induced average moment which explains the static susceptibility. Secondly, our results suggest that the Ce form factor has a different spatial extent from that found for other Ce compounds with larger Ce–Ce separations. This could imply a significant Ce 5d-electron contribution to the density of states at the Fermi surface, although the 5d spectral weight at the Fermi surface has been determined to be small in band-structure calculations. The extent of the Ce form factor agrees well with an alternative scenario, in which there is no d-electron contribution, but the orbital component of the 4f form factor is quenched. We hope that our measurements will stimulate more elaborate calculations of the magnetization density, facilitating further examination of these two possibilities.

No significant change in the magnetic density distribution with temperature was detected, even in the superconducting state. The latter result is probably indicative of significant spin–orbit scattering which could be related to the presence of an imperfect flux-line lattice.

References

[1] Huxley A, Dalmas De Réotier P, Yaouanc A, Caplan D, Couach M and Lejay P 1996 *Phys. Rev.* B **54** 9666
[2] Nakama T, Hedo M, Maekawa T, Higa M, Resel R, Sugawara H, Settai R, Onuki Y and Yagasaki K 1995 *J. Phys. Soc. Japan* **64** 1471
[3] Palenzona A 1991 *J. Alloys Compounds* **176** 241
[4] Yang S H, Kumigashira H, Yokoya T, Chainani A, Takahashi T, Takeya H and Kadowaki K 1996 *Phys. Rev.* B **53** 11 946
[5] Sereni J 1994 *J. Alloys Compounds* **207** 229
Sereni J and Kappler J P 1994 *J. Phys.: Condens. Matter* **6** 4771
[6] Lopez-Aiguilar F, Balle S and Costa-Quintana J 1988 *Phys. Rev.* B **38** 163
[7] Costa-Quintana J, González-León, Lopez-Aiguilar F, Puig-Puig L and Sánchez-López M M 1995 *Physica* B **206** 186
[8] Yanese A 1986 *J. Phys. F: Met. Phys.* **16** 1501
[9] Higuchi M and Hasegawa A 1996 *J. Phys. Soc. Japan* **65** 1302
[10] Hedo M, Inada Y, Ishida T, Yamamoto E, Haga Y, Onuki Y, Higuchi M and Hasegawa A 1995 *J. Phys. Soc. Japan* **64** 4535
[11] Huxley A, Paulsen C, Laborde O, Tholence J L, Sanchez D, Junod A and Calemczuk R 1993 *J. Phys.: Condens. Matter* **5** 7709
[12] Kadowaki K, Takeya H and Hirata K 1996 *Phys. Rev.* B **54** 462
[13] Yagasaki K, Hedo M and Nakama T 1993 *J. Phys. Soc. Japan* **62** 3825
[14] Sugawara H, Sato H, Yamazaki T, Kimura N, Settai R and Onuki Y 1995 *J. Phys. Soc. Japan* **64** 4849
[15] Dilley N R, Herrmann J, Han S H, Maple M B, Spagna S, Diederichs J and Sager R E 1996 *Physica* C **256** 150
[16] Modler R, Gegenwart P, Lang M, Deppe M, Weiden T, Lühman T, Geibel C and Steglich F 1996 *Phys. Rev. Lett.* **76** 1292
[17] Sato H, Kobayashi Y, Sugawara H, Aoki Y, Settai R and Onuki Y 1996 *J. Phys. Soc. Japan* **65** 1536
[18] Goshima H, Suzuki T, Fujita T, Settai R, Sugawara H and Onuki Y 1996 *Physica* B **224** 172
[19] Steglich F, Modler R, Gegenwart P, Deppe M, Weiden M, Lang M, Geibel C, Luhmann T, Paulsen C, Tholence J L, Onuki Y, Tachiki M and Takahashi S 1996 *Physica* C **263** 498
[20] Onuki Y *et al* 1996 *Physica* B **224** 28
[21] Huxley A, Cubitt R, McPaul D, Forgan E, Nutley M, Mook H, Yethiraj M, Lejay P, Caplan D and Pénisson J M 1996 *Physica* B **223** 169
[22] Roy S 1992 *Phil. Mag.* B **65** 1435
[23] Fulde P and Ferrel R 1964 *Phys. Rev.* **135** 550
[24] Larkin A and Ovchinnikov Yu N 1965 *Sov. Phys.–JETP* **20** 762
[25] Takahashi S, Tachiki M, Modler R, Gegenwart P, Lang M and Steglich F 1996 *Physica* C **263** 30
[26] Tachiki M, Takahashi S, Gegenwart P, Weiden M, Lang M, Geibel C, Steglich F, Modler R, Paulsen C and Onuki Y 1996 *Z. Phys.* B **100** 369
[27] Suzuki T, Goshima H, Sakita S, Fujita T, Hedo M, Inada Y, Yamamoto E, Haga Y and Onuki Y 1996 *J. Phys. Soc. Japan* **65** 2753
[28] Stassis C, Arthur J, Majkrzak C F, Axe J D, Batlogg B, Remeika J, Fisk Z, Smith J L and Edelstein A S 1970 *Phys. Rev. Lett.* **24** 1415
[29] Wilson A J C (ed) *International Tables for Crystallography* vol C (Dordrecht: Kluwer Academic)
[30] Papoular R J and Gillon B 1990 *Neutron Scattering and Data Analysis Conf. (Didcot, 1990) (Inst. Phys. Conf. Ser. 107)* (Bristol: Institute of Physics Publishing) p 101
[31] Lovesey S 1987 *Theory of Neutron Scattering from Condensed Matter* (Oxford: Oxford University Press)
[32] Freeman A J and Desclaux J P 1979 *J. Magn. Magn. Mater.* **12** 11
[33] Boucherle J X and Schweizer J 1985 *Physica* B **130** 337
[34] Gignoux D, Givord F, Lemaire R and Tasset F 1982 *J. Physique Coll.* **43** C7 257
[35] Shull C G and Wedgwood F A 1966 *Phys. Rev. Lett.* **16** 513
[36] MacLaughlin D E 1977 *Solid State Physics* vol 31 (New York: Academic) p 1
[37] Ishida K, Mukuda H, Kitaoka Y, Asayama K and Onuki Y 1996 *Z. Naturf.* a **51** 793
[38] Matsuda K, Kohori Y and Kohara T 1995 *J. Phys. Soc. Japan* **64** 2750
[39] Stassis C *et al* 1986 *Phys. Rev.* B **34** 4382
[40] Anderson P W 1959 *Phys. Rev. Lett.* **3** 325
[41] Fulde P and Maki K 1965 *Phys. Rev.* **139** A788